nature portfolio

https://doi.org/10.1038/s41586-021-04260-1

Supplementary information

Ferroelectric incommensurate spin crystals

In the format provided by the authors and unedited

Supplementary Information - Howie-Whelan 2-beam diffraction contrast simulation of polarisation vortex structures in $PbTiO_3$

Dorin Rusu[1], Jonathan J. P. Peters[1,2], Thomas P. A. Hase[1], James A Gott[1], Gareth A. A. Nisbet[3], Jörg Strempfer[4], Daniel Haskel[4], Samuel D. Seddon[1], Richard Beanland[1], Ana M. Sanchez[1] and Marin Alexe[1]

[1]*Department of Physics, University of Warwick, Coventry, CV4 7Al, United Kingdom*

[2] *School of Physics, Trinity College Dublin, Dublin, Ireland*

[3]*Diamond Light Source, Didcot, OX11 0DE, United Kingdom*

[4]*Argonne National Laboratory, Lemont, IL 60439, United States of America*

1. Mechanisms giving rise to diffraction contrast

The displacements around a vortex give rise to diffraction contrast in two distinct ways. First, the lattice strain produces a change in crystal orientation and a local change in the deviation parameter s, which describes the proximity of the crystal to the Bragg condition employed for imaging. The contrast in TEM images produced by the local tilt of the crystal is familiar from images of dislocations and can be modelled as a local change in s,

$$ds = \frac{d(\mathbf{g}.\mathbf{R})}{dz} \qquad (1)$$

where **g** is the diffraction vector, $\mathbf{R}$ is the displacement of the crystal from an ideal, unstrained lattice, and the electron beam is propagating along z. The second contrast mechanism arises from the relative displacements of the atoms on a sub-unit cell scale, which changes the structure factor F_g:

$$F_g = \sum_j f_j \exp\left(2\pi i \mathbf{g}.\mathbf{r}_j\right) \qquad (2)$$

where the sum is performed for all atoms in the unit cell and f_j is the scattering factor for atom j with fractional coordinates $\mathbf{r}_j$. This results in a local change in the extinction distance ξ_g:

$$\xi_g = \frac{\pi V_c k \cos\theta_g}{F_g} \qquad (3)$$

where V_c is the volume of the unit cell, k is the magnitude of the electron wave vector and θ_g is the Bragg angle.

These equations are well-known and can be found in textbooks such as Hirsh et al.[1], Williams and Carter[2] and many more. In our model we follow a simplified version of the approach taken by Head et al.[3] in which the parameters s and ξ_g are a function of position, $s(x,y,z)$ and $\xi_g(x,y,z)$. These feed into the two-beam Howie-Whelan equations, which can be used to calculate the electron amplitude as the wave propagates through the crystal. Using the column approximation, which assumes that for any given pixel in the image we may neglect any scattering from/to adjacent pixels, we may divide the material into a set of slices and use the electron amplitude as calculated from the Howie-Whelan equations for one slice as the input to the next, until the exit surface of the crystal is reached. At the exit surface, the bright field (BF) and dark field (DF) intensity can then be calculated. This has been implemented using Python/C++ code running on a GPU using pyOpenCL (see https://github.com/WarwickMicroscopy/Howie-Whelan_Polarisation-vortex), with scattering factors from Kirkland[4]. Although a full many-beam simulation is required for accurate results, the simple two-beam calculation is expected to be correct to first order, apart from weak-beam imaging conditions where coupling into a third beam changes intensities very significantly.

2. The structure to be simulated

Cross section ac-STEM images of the PbTiO3 (PTO) layer embedded between $SrRuO_3$ (SRO) layers show vortex structures running along [100] (SI Figure 1). Adjacent vortices have opposite senses, clockwise & anticlockwise, and have a spacing between 6 and 8nm in SI Figure 1. The PTO layer is 5.25nm (13 unit cells) thick and the SRO above and below is 4.4nm (11 unit cells) thick. There is a 4nm $DyScO_3$ (DSO) layer below the SRO and a $SrTiO_3$ substrate.

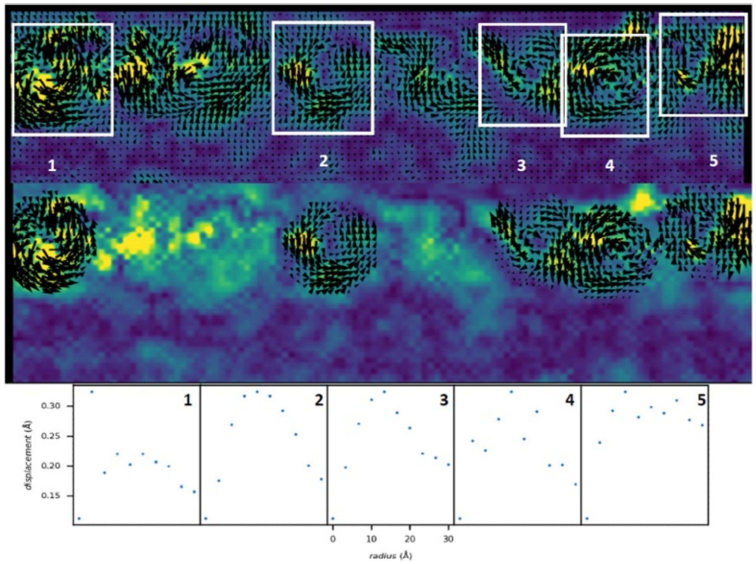

SI Figure 1 | Vortices seen in cross section.

Plan view dark field TEM shows a striped labyrinthine structure with a slight additional modulation along the stripes that may be caused by additional cycloidal or helical distortions (SI Figure 2). The spacing of the stripes is about 10nm – this is slightly bigger than that in SI Figure 1 but presumably we have one dark (or bright) stripe per vortex, and vortices of opposite senses give the same contrast. Contrast is quite strong; for the dark field (DF) **g** = 110 images it is around 25% and for DF **g** = 100 images it is around 50%.

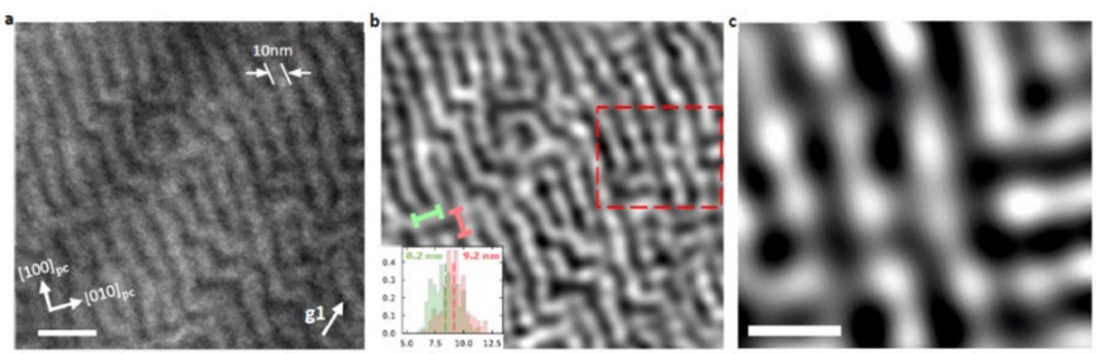

SI Figure 2 | Vortices seen in plan-view using diffraction contrast imaging.

From SI Figure 1, the sub unit-cell displacements around a vortex are a maximum at about 5-6 unit cells from the vortex core and have a magnitude there of about 0.033 nm. We can fit the magnitude of the displacement, R, as a function of distance from the vortex core, d, using a model of the form

$$R = A\, d^n \exp(-\alpha d^n) \tag{4}$$

where R is perpendicular to d. This function can be matched to the data using the three fitting parameters A, n and α. A fit to the data in panel 2 of SI Figure 1 is shown in SI Figure 3 with A =0.055, n =1.15 and α =0.6.

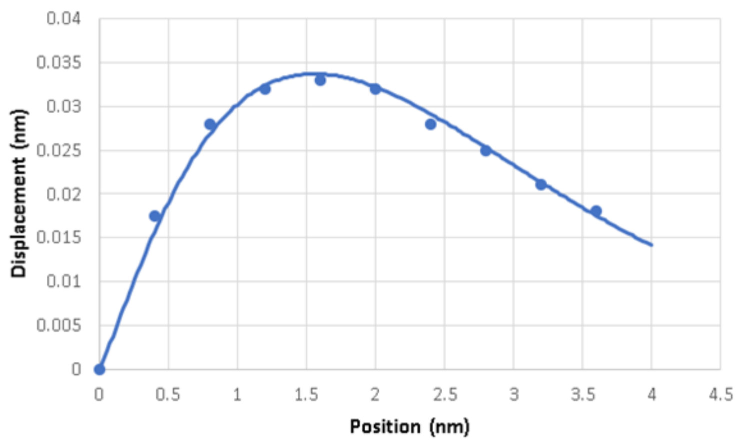

SI Figure 3 | Fit to experimental polarisation displacements (SI Figure 1 - panel 2) using Eq.(4) with $\mathrm{A} = 0.055$, $\mathrm{n} = 1.15$ and $\alpha = 0.6$

In addition to the sub-unit cell displacements there is lattice strain. Although in the sample examined here these displacements can vary from place to place, we use a simple vortex of the same form as given in equation (4), with a displacement field perpendicular to the free surface as shown in SI Figure 4. Although this does not take into account the relaxation that takes place due to the presence of the free surfaces of the TEM specimen, we expect that it is sufficiently close to reproduce the essential features of the images.

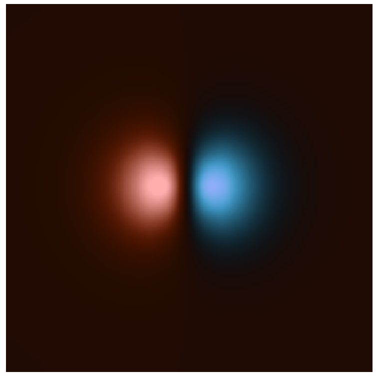

SI Figure 4 | The ε_{xx} strain component for a vortex.

We use n =1.15 and α =0.6, but a magnitude of A =0.03, which gives a maximum strain of 0.018 perpendicular to the electron beam, similar to that measured from geometric phase analysis of ac-STEM images.[5] (https://jjppeters.github.io/Strainpp/)

3. Results

We first consider the case where there is no strain in the material and the only contribution is due to the sub-unit cell (polarisation) displacements. The vortices are 7nm below the surface of the sample. The thickness of the specimen is not known but if it has just the top three layers it is 4.4+5.25+4.4 = 14nm thick. We neglect the difference in scattering of the SRO above and below the PTO layer. As shown in SI Figure 5 all vortices have the same contrast irrespective of sign, and appear as a diffuse band of dark contrast. However, the contrast is extremely low and is essentially invisible in the simulation (SI Figure 5 left, in which vacuum has intensity zero and the maximum intensity in the image has unit intensity). The plot (SI Figure 5 right) gives the calculated intensity in absolute units (intensity of the incident beam = unity) and the contrast can be calculated as roughly 0.5%. This is extremely small and the lines of are only visible in an image with enhanced contrast (SI Figure 5 centre). There is zero contrast when the diffraction vector **g** is parallel to the vortex line direction.

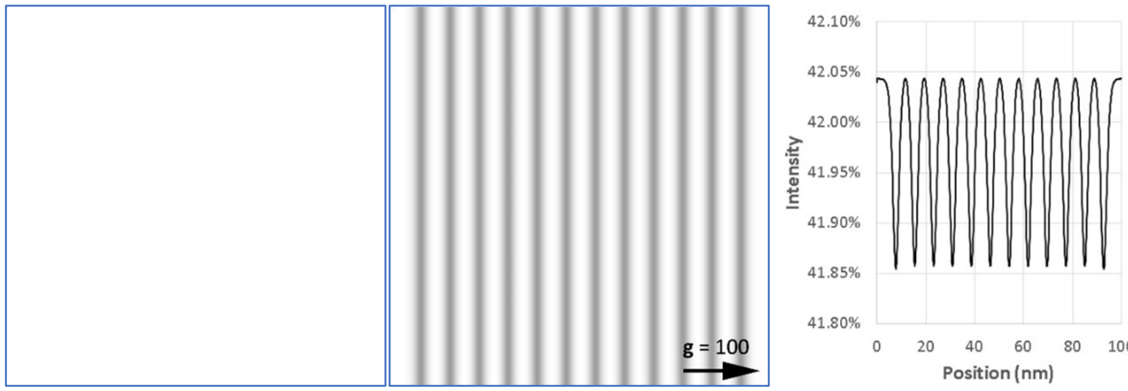

SI Figure 5 | Simulated diffraction contrast **g** = 100, s = 0 dark field image of an array of polarisation vortices (no strain) running along [010] (vertically), with spacing 8nm and sub-unit cell displacements described by Eq.4 with $\mathrm{A} = 0.055$, $\mathrm{n} = 1.15$ and $\alpha = 0.6$ in a 14nm thick plan-view specimen. The field of view is 100x100 nm. Left: without contrast enhancement the vortices are essentially invisible; centre: with contrast enhancement; right: absolute intensity plot.

Although the contrast changes (and can even reverse) depending upon specimen thickness, diffraction vector **g** and deviation parameter s, this does not change its strength sufficiently to allow polarisation to be visualised in diffraction contrast TEM or 4D-STEM. We may thus conclude that polarisation is essentially invisible in diffraction contrast TEM images. We also note that the same argument applies to 4D-STEM measurements, where the intensity in a diffraction pattern is mapped over a scanned area, with the caveat that multiple scattering near a zone axis makes unequivocal interpretation of this contrast rather more difficult.

We now consider strain contrast and give a simulated image in SI Figure 6 for an array of vortices with strain ($A = 0.03$, $n = 1.15$ *and* $\alpha = 0.6$) using **g** = 100, but with the parameter s varying from top to bottom of the image. This corresponds to a crystal that bends through the Bragg condition and shows how the contrast varies due to this effect. Here the contrast is very strong, which would make the vortices readily visible experimentally. However, we see that clockwise and anticlockwise vortices have different contrast. When s is positive and the vortex has anticlockwise displacements when viewed along [100] the contrast is weak, whereas for clockwise displacements the contrast is strong. This strong/weak contrast reverses for opposite signs of s and **g**. There is zero contrast when the diffraction vector **g** is parallel to the vortex line direction.

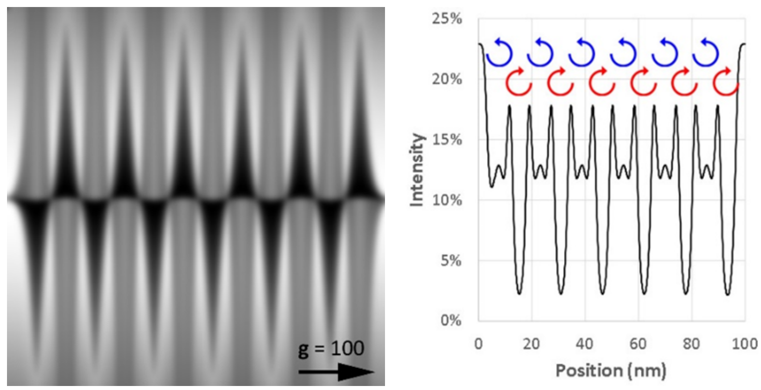

SI Figure 6 | Simulated diffraction contrast $\mathbf{g}$ = 100 dark field image of an array of vortices running along [010] (vertically), with spacing 8nm and deformation field described by Eq.4 with $\mathrm{A} = 0.03$, $\mathrm{n} = 1.15$ and $\alpha = 0.6$ in a 14nm thick plan-view specimen. Contrast is due to local strain and the field of view is 100x100 nm. Left: image with a deviation parameter s varying vertically (the exact Bragg condition at s =0 is half way up the image). Clockwise and anticlockwise vortices give different contrast, which depends on s, illustrated by the plot on the right for s =0.01 nm.

As noted in section 1, the two-beam simulation is unreliable for large deviations from the Bragg condition, i.e. at the top and bottom of SI Figure 6 where weak-beam conditions apply. By analogy with dark field weak-beam images of the strain field of a dislocation, we would expect the actual contrast here to become a sharp bright line. This does not change the invisibility of the vortices when $\mathbf{g}$ is parallel to their line direction.

Adding a modulation of the displacement magnitude along the vortex changes the width of the line of contrast as shown in SI Figure 7. This also tends to even up the contrast between vortices of different chirality. However, it doesn't change the direction of the stripes and the vortices still have no contrast when the diffraction vector $\mathbf{g}$ is parallel to their line direction.

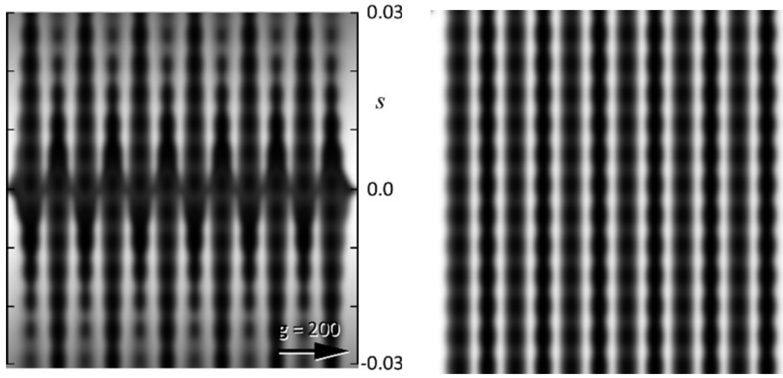

SI Figure 7 | Simulated diffraction contrast **g** = 100 dark field image of an array of vortices running along [010] (vertically), with spacing 8nm and deformation field described by Eq.4 with $\mathrm{A} = 0.03$, $\mathrm{n} = 1.15$ and $\alpha = 0.6$, plus a sinusoidal variation of 10%, in a 14nm thick plan-view specimen. Contrast is due to local strain and the field of view is 100x100 nm. Left: image with a deviation parameter s varying vertically (the exact Bragg condition at s =0 is half way up the image). Right: image with constant s =0.01 nm.

The modulation of SI Figure 7 does not produce a very good match to the experimental images (Extended data SI Figure 9), in which images taken with **g** = 100 or **g** = 010 give lines of contrast of fairly constant width. The double modulation we observe is only present when **g** = 110. We may thus exclude a modulation of the helical component of displacement.

Experimentally we observe lines of contrast in both [100] and [010] directions that each become invisible when **g** is parallel to their line direction. SI Figure 8 shows that clockwise and anticlockwise vortices can have different contrast and their crossing can increase or decrease contrast, depending upon their sign.

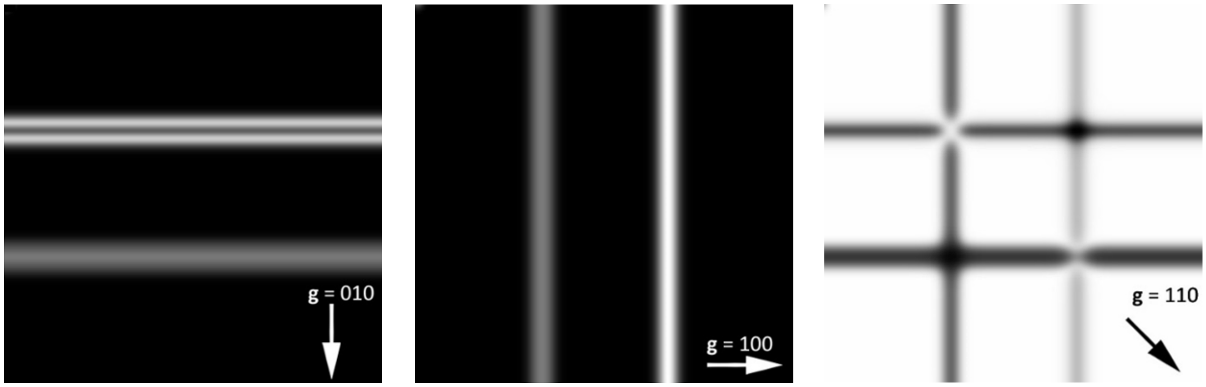

SI Figure 8 | Simulated diffraction contrast **g** = 100, 010 and 110 dark field images of two widely-spaced arrays of vortices running along [010] (vertically) and [100] (horizontally), and deformation field described by Eq.4 with $\mathrm{A} = 0.03$ (vertical), $\mathrm{A} = 0.15$ (horizontal), $\mathrm{n} = 1.15$ and $\alpha = 0.6$. Contrast is due to local strain and the field of view is 100x100 nm.

For closely spaced vortices (SI Figure 9), the lines of contrast may overlap. There is some resemblance to the experimental images.

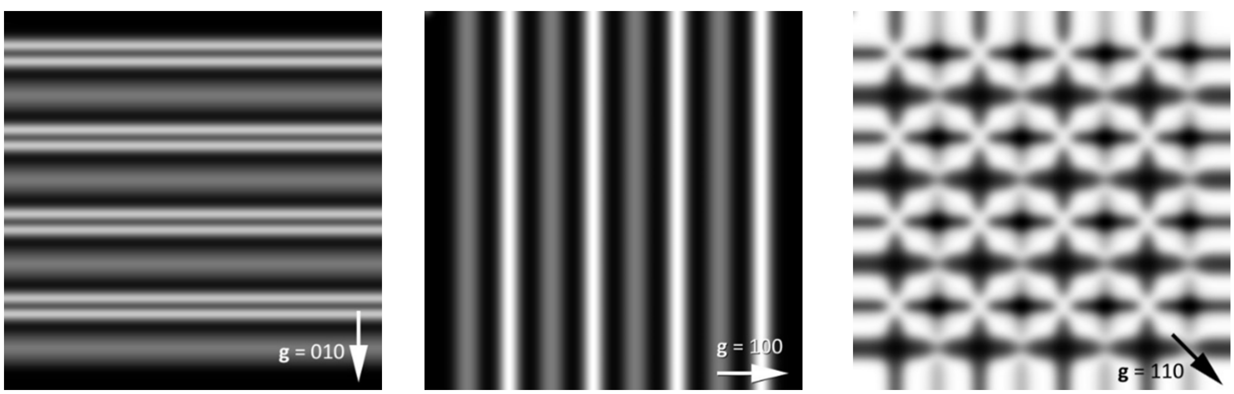

SI Figure 9 | Simulated diffraction contrast **g** = 100, 010 and 110 dark field images of two widely-spaced arrays of vortices running along [010] (vertically) and [100] (horizontally), and deformation field described by Eq.4 with $\mathrm{A} = 0.03$ (vertical), $\mathrm{A} = 0.15$ (horizontal), $\mathrm{n} = 1.15$ and $\alpha = 0.6$. Contrast is due to local strain and the field of view is 100x100 nm.

4. Summary

Two-beam diffraction contrast simulations reproduce some aspects of the experimentally observations. Most importantly they confirm that a vortex becomes invisible when the **g**-vector is perpendicular to their displacements. Also, they show that strain contrast is much stronger than polarisation contrast. However, they fail to reproduce the observations exactly, due to the limitations of the two-beam calculation and uncertainty about the detail of the displacement field. A more accurate simulation would require the inclusion of multiple scattered beams, which may allow a comparison between different models of the displacement fields in this double-modulated structure.

Supplementary Information references

1. Hirsch, P.B., Howie, A., Nicholson, R.B., Pashley, D.W. & Whelan, M.J. Electron Microscopy of Thin Crystals (Butterworths, London; 1965).
2. Carter, C.B. & Williams, D.B. Transmission electron microscopy: Diffraction, imaging, and spectrometry. (Springer, 2016).
3. Head, A., P, H., LM, C., AJ, M. & CT, F. Computed electron micrographs and defect identification. (North Holland, 1973).
4. Kirkland, E.J. Advanced computing in electron microscopy. (Springer, 1998).
5. Peters, J. https://jjppeters.github.io/Strainpp/ (2017).